Real-time processing methods to characterize streamwise vortices

Caroline Braud, Alex Liberzon

Real-time processing methods to characterize streamwise vortices

Caroline Braud*

LHEEA Laboratory (ECN/CNRS), 1 rue de la Noë, 44000 Nantes, France

Alex Liberzon*

School of Mechanical Engineering, Tel Aviv University, 69978 Tel Aviv, Israel

Abstract

One of the bottlenecks of an active control of turbulent boundary layers based on particle image velocimetry (PIV) measurements relates to the ability to process PIV images and extract useful for control information in real-time, on a time scale relevant for the selected control strategy. We propose two methodologies to extract useful information from PIV measurements in the $y-z$ spanwise - wall normal cross-section, based on characterisation of properties such as size and strength of streamwise vortices. The vortices are created by active vortex generators embedded in a fully turbulent boundary layer. The proposed methodologies combine vortex identification and characterisation methods that use instantaneous PIV realisations to extract centers and strengths of streamwise vortices. The main purpose is to compare a standard vortex identification method that provides a robust and accurate estimate with another, ad-hoc method that is less robust or accurate but has a large computational speed gain potential. For demonstration purposes we use PIV measurements obtained at the wind tunnel facility downstream active vortex generators[1, 2]. The first algorithm uses the Q-criteria and the integration of vorticity of each extracted vortex. This robust and accurate method requires the full spatially resolved PIV field followed by the computationally expensive spatial derivatives calculations

*Corresponding author
Email address: caroline.braud@ec-nantes.fr (Caroline Braud)

and an integration. The second algorithm utilises the prior knowledge about the presence and shape of streamwise vortices expected in the measurement, therefore uses only a single line velocity profile estimate and can be parallelized to obtain few horizontal velocity profiles at different wall-normal distances. We compare the two methods and discuss their potential in term of computation times and robustness. Results show that in a turbulent boundary layer, a moving window average of a number of instantaneous fields is needed for both methods.
Keywords: `active vortex generator, particle image velocimetry, vortex identification, boundary layer control`

1. Introduction

Vortex generators (VGs) – devices generating streamwise vortices which bring high momentum fluid near the surface such that it delays the apparition of flow separation – are widely used to control separation in turbulent boundary layers, as reviewed by Lin [3]. Active devices that reproduce streamwise vortices by blowing jets from the wall, rapidly replace the passive VGs, mainly because of the high potential for use in feedback based control loops [4]. High shear from the jet edges induces a roll-up of the boundary layer flow [5] and this jet-free stream interaction leads to a pair of counter-rotating streamwise vortices generated behind a single jet blown perpendicular to the wall. When the jet has an angle to the wall (pitch and/or skew angle), two counter-rotating vortices are initially created downstream of the device and evolve rapidly into a single coherent vortex of one sign accompanied by a much smaller and weaker region of circulation of the opposite sign near the wall [6]. Properties of the generated vortex, such as circulation, distance to the wall and size, among others, dictate the efficiency of the boundary layer separation control.

Sensors used in feedback loops, such as pressure sensors [7], hot-film sensors [4] and similar, are typically installed at the wall. However, sensing of flow properties at the wall is not adapted to detect vortex properties which are of crucial importance for the boundary layer control. Sensing methods based

on flow measurements above the wall using particle image velocimetry (PIV) have been recently demonstrated for closed-loop control using low Reynolds benchmarks [8, 9]. The control objective in these studies was to re-attach the flow using the vortex structures from the Kelvin-Helmholtz instability of the separated flow region. However, once attached, it is impossible to control the flow until the flow separates again and new vortex structures appear in the flow.

We propose to develop real-time processing methodologies to characterise the streamwise vortex properties resulting from the active jets/turbulent boundary layer interaction. There exist different methods to identify vortices. The most popular ones are methods based on the velocity gradient tensor such as the Q-criterion [10], the Δ-criterion [11], the λ_2-criterion [12]. Chakraborty et al. [13] have shown that all these methods are approximately equivalent. These are Galilean invariants, that enable to distinguish swirling motion from shearing motion. These methods were however developed in the perspective to help in the analysis of turbulent flows, but not in the perspective of closed-loop implementation. The purpose of this work is to explore the methods to extract information useful for feedback-loop control applications from PIV data. Two methods are proposed to identify and characterise streamwise vortices strength, created downstream active jet devices embedded in a turbulent boundary layer flow. The first method is using the well known Q criterion [10]. The second one is an ad-hoc method based on prior knowledge of streamwise vortices presence and orientation. It uses a direct estimation of the vortex strength from a horizontal profile of a single vertical velocity component. It allows us to use the method in parallel, strongly integrated with the PIV correlation analysis

The paper is organized as follows. First, we present the measurements and the obtained experimental database used in this paper in the Section 2. The relevant times for processing PIV data for closed-loop implementation (i.e. in real time) are briefly recalled in the Section 3. The two algorithms to identify the generated streamwise vortices and extract their properties necessary for the feedback loop are described in Sections 4 and Sections 5. Finally, we compare the two methods and discuss the limitations in the proposed methods in Sections 6,

followed by conclusions in Section 7.

2. Experiment and the database

We develop our algorithms based on the empirical results, obtained using stereoscopic PIV (SPIV) experiment performed in the LML wind tunnel facility. In this experiment active vortex generators (AVGs) were embedded in a highly turbulent boundary layer. Details on the wind tunnel facility, control set-up and SPIV measurements can be found in [1, 2] and only briefly repeated below for the sake of completeness. Use of the stereoscopic setup was important for the accurate measurement of the streamwise vorticity in the spanwise - wall-normal plane.

2.1. Wind tunnel

The turbulent boundary layer which develops in the LML wind tunnel is extensively described and characterized in Carlier et al. [1]. The working section is 1 m high, 2m wide and 21.6 m long. The boundary layer thickness that develops in the test section is $\delta = 0.3$ m at the free-stream velocity $U_\infty = 8.5$ m/s and does not change much throughout the test section. The turbulence level in the free stream is about 0.3% of U_∞ , and the temperature is kept within $0.2C^\circ$ by use of an air-water heat exchanger in the plenum chamber [1].

2.2. Active vortex generators

A transverse line of active devices was set in the test section by drilling holes at the wall with an angle to the wall of 45° and an angle to the free stream of 45° as schematically shown in figure 1. Active devices were arranged in a counter-rotating configuration (the angles to the wall are 45° and -45° for devices composing the pair), so that three pairs can fit in the transverse direction of the section test. The distance between devices within a counter-rotating pair is fixed to $15D_j$ where $D_j = 10$ mm is the jet diameter. The distance between

pairs is $33.6D_j$. Three jet velocity ratios were tested, $VR = V_j/U_\infty = 3, 4, 5$ with V_j the jet exit velocity. The momentum coefficient is given by

$$C_\mu = \frac{Q_m V_j}{P_\infty S} \tag{1}$$

where Q_m is the mass flow rate, P_∞ the dynamic pressure, S the total surface that is controlled (including areas between jets). For incompressible controlled jets, which is the case in the present experiments, this is proportional to VR:

$$C_\mu = \frac{2S_j}{S} VR^2 \tag{2}$$

with $S_j = n\pi D_j^2$ the total surface of controlled jets with $n = 4$ the number of jets. The ratio VR will thus be used instead of C_μ in the following. The air circuit which was used to provide compressed air to the actuators is composed of a compressor, a filtration system, a proportional valve, two volumetric flow meters, a manometer, a thermometer and a large reservoir of 90 liters. More details on the air circuit arrangement can be found in Ref. [4].

2.3. SPIV measurements

This article presents an experimental investigation of the flow in the same facility, with the same turbulent boundary layer, and most importantly with the same experimental setup (same PIV equipement and parameters such as magnification, lens aperture ...) as Foucaut et al (2014) [2]. Only the flowfield was different because the active device were replaced by passive devices, but the setup was kept identical (in fact the two experiments were conducted just one after another). We repeat the description here for the sake of clarity. In order to obtain a larger field of view, two stereoscopic PIV systems were used. Each system is based on Hamamatsu 2K $\times$ 2K pixel cameras equipped with micro Nikkor 105 mm lenses at f# 5.6. The field of view of each system is about 42 $\times$ 28 cm^2 (corresponding to about $1.5\delta \times \delta$ where δ is a boundary layer thickness). The field of view of two systems in Scheimpflug condition [14] was adjusted to approximately 72 $\times$ 28 cm^2 ($2.3\delta \times \delta$), and the grid spacing is 2.3 mm which corresponds to 40 wall units (or 0.0076δ). The seeding was

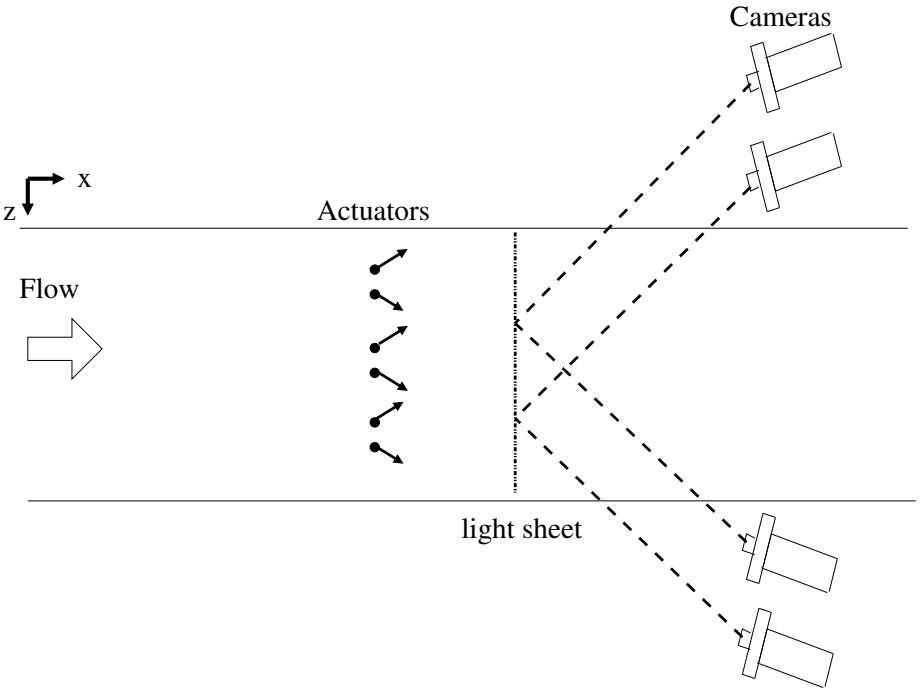

Figure 1: Stereoscopic PIV set-up. Two SPIV systems were used to increase the field of view and resolution of the measurements.

poly(ethylene glycol) micron particles of $d = 1\mu$m, generated by Laskin nozzle. The particle image size appears to be of the order of 1.5 pixel. When the particle images are discretized on more than one pixel, the displacement peak from the correlation of images can be fitted (typically a 3 points Gaussian fit) in order to retrieve the displacement with sub-pixel accuracy[15]. Also, with actuators, the local gradient in the interrogation window size of our experiments is around the same order of magnitude of the size of the particle, so that the amplitude of the correlation peak decreases but its location is unchanged [16]. The laser used is a BMI YAG system with 2 cavities which is able to produce energy of 220 mJ per pulse at a frequency of 12 Hz. A mirror is stuck under the bottom glass in order to reflect the light in the wind tunnel and increase the light intensity. The beam waist, located at the wall, was measured by means of burning paper,

to be of the order of 1 mm. To get such a thick waist, a spherical lens of 5 m focal length was used. The optimal time interval $\Delta t = 90\mu$s and the separation of the two light sheets in the streamwise direction, 0.5 mm, were determined following the procedure described in Ref. [2] to create a sufficient out-of-plane displacement of particles and increase the dynamic range of the measurements.

The in-house code developed by the LML implements the 3D warping technique with back-projection/reconstruction as suggested by Soloff et al. [17]. It means that the PIV evaluation is first performed in the image space of each camera, using an FFT based multi-pass and multi-grid cross-correlation algorithm [18, 19, 20]. The SPIV images were cross-correlated in three steps in the image plane of each camera, starting with an interrogation window of 64×64 px and down to 32×32 px with an overlap of 50% between adjacent interrogation windows. This cross-correlation is performed on a mesh defined as the forward projection of a Cartesian grid in the object space [21]. The position of the correlation peak is detected using two one-dimensional Gaussian fits. It should be noted that this step is performed before back-projection in the 2D2C velocity field, so that the out-of-plane projection of the streamwise velocity component is added to the in-plane velocity components, which improves the correlation peak detection. The back-projection of the two 2D-2C velocity fields in the object space and the three component reconstruction are realised in a single step using the method of Soloff et al. [17]. The model used to map the object volume to the image plane is a polynomial with cubic dependence in the two in-plane directions and quadratic in the out-of-plane direction. The coefficients of the polynomials are obtained using images of a planar calibration target translated in the out-of-plane direction. Finally a misalignment correction is performed, as implemented in Coudert and Schon [21].

Foucaut et al (2014) evaluated the setup accuracy using two methodologies. First, through a comparison of the PIV measurements in the turbulent boundary layer canonical configuration (without actuators) against hot-wire measurements. The PIV errors in the in-plane motion (with displacements below 1 pixel) were evaluated by comparing these two measurement techniques and found of

the order of 0.1 - 0.2 px. This first step validates that the set-up (particle diameter, concentration, alignment etc ...) is able to obtain a high accuracy. Then, errors were evaluated for the non-canonical flow configuration (with passive actuators), using the overlapping region of the two stereoscopic field acquired simultaneously. In the paper of Foucaut et al (2014), an accuracy of 0.15 px for u and w and 0.1 px for v was obtained. Following the same approach, the accuracy of the present study was computed with active actuators, and led to the error of w up to 5% of the free-stream velocity (corresponding to 0.15 px) and which reaches 9% of the free-stream velocity close to the wall (for $y < 0.1\delta$). The error on the wall normal component, v, was found very similar with and without actuators, around 0.1 px. Regarding the peak locking, due to the image size of the particle (whatever the flow configuration), Foucaut et al (2014) have demonstrated a very low effect of it in the present set-up.

3. Relevant times for processing PIV data

In a closed loop system, the sensing system has to extract a relevant information at every control step. In our case, the relevant information is an estimate of the circulation from a PIV field. Therefore, at every control step, one should do a PIV analysis, an identification and a characterisation of the streamwise vortices and an estimate of the circulation. The relevant hardware and software time consuming steps can be listed as follows:

1. the time interval between PIV realisations, i.e. reciprocal of the PIV acquisition frequency
2. the time required to process PIV images,
3. the time needed to extract useful information, i.e. vortex circulation (Γ) in the present case.
4. the delay time of a control loop (in the case of simple proportional controller there is no time delay)

The proposed real time processing methods correspond to the second and third items which carry the highest computational cost. The first real time vortex

characterisation method presented in the present work (see Section 4) is used as a reference time scale case to extract vortex circulation from the velocity field. The second proposed method based on the vertical velocity profile is impacting two computational cost: the time to process PIV images and the time to extract vortex properties (see Section 5).

4. Characterisation method based on Q criterion

Our main goal is to develop methods that identify streamwise vortices in PIV wall-normal spanwise flow fields v, w and characterise their properties (position, size and circulation, Γ). The first method is based on a well-known Q criterion and it will serve as a baseline for the comparison of robustness, accuracy and computational time.

4.1. Demonstration of the method

We first demonstrate the vortex identification method using a smooth flow field with vortices. For the sake of demonstration we use an average flow field obtained from an ensemble of 100 PIV realizations in which vortices due to active vortex generators are clearly seen and the signal-to-noise ratio is high. Then we proceed to modify the proposed method to detect vortices and estimate their properties in instantaneous PIV realisations.

The important parameters are a) position of its center, y_0, z_0 b) size, R, c) circulation, Γ. These properties can be extracted from PIV realisations based on vorticity and the Q criterion [13]. We propose to implement this algorithm using steps described in the diagram in the following figure 2, starting from spatial velocity gradients, $\partial v/\partial y, \partial v/\partial z, \partial w/\partial y, \partial w/\partial z$:

First, the gradients in transverse and wall-normal (y, z) directions are computed from the two-dimensional PIV realisations from which the longitudinal vorticity $\Omega_x(y, z)$, the rate-of-strain tensor and the Q-criterion in 2D (without $\partial(.)/\partial x$, $(.) = u, v, w$) are obtained:

$$\Omega_x(y, z) = \frac{dw}{dy} - \frac{dv}{dz} \tag{3}$$

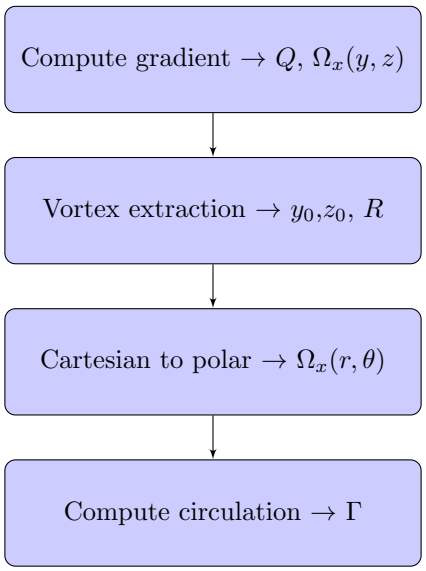

Figure 2: Diagram of the algorithm developed to extract the vortex properties (localization (y_0, z_0), radius R and circulation Γ), of produced vortices behind active vortex generators.

$$Q = \frac{1}{2}\left[||Rot_{ij}||^2 - ||Str_{ij}||^2\right] \tag{4}$$

with $||Rot_{ij}|| = \frac{1}{2}(\partial u_i/\partial x_j - \partial u_j/\partial x_i)$ the rotation rate tensor and $||Str_{ij}|| = \frac{1}{2}(\partial u_i/\partial x_j + \partial u_j/\partial x_i)$ the strain rate tensor.

We estimate the uncertainty of velocity gradients using the method proposed in [22]. For instance, the uncertainty of $\Omega_x(y,z)$ computed using the central difference scheme is estimated according to Eq. (3):

$$\delta{\Omega_x}^2 = 2\left(\frac{1}{2d}\right)^2 [1-\rho(2d)](\delta v^2 + \delta w^2)$$

where $\delta v = 0.1$ and $\delta w = 0.15$ are the displacement uncertainty for the velocity components, $d = 16pix$ is the grid spacing and $\rho = 0$ (i.e. maximizing the error) is the cross-correlation of the error. The uncertainty propagates from velocity components to the uncertainty of $\delta\Omega_x = 0.008$ which refers to approximately 20% of the lowest vorticity peaks.

Once the vorticity and the Q-criterion are computed, we find the vortex center (y_0,z_0) using the maximum of Q. Although the radius R is first estimated using the maximal distance between two close zero-crossing points of vorticity, the vortex core size is obtained based on maximal azimutal velocity. The vorticity field with higher uncertainty is therefore not used as a direct measure of the radius, but rather as an initial marker of four streamwise vortices in the PIV field. Note that due to the use of Q in two-dimensional approximation only, the vortex center position requires an additional refining iteration. Also, by this procedure described in the following, the uncertainty on the location of the vortex center is reported at the level of the uncertainty of the velocity components.

In the presence of a vortex, like the one shown in figure 3, an horizontal line of the velocity field at the vortex center will contain mainly the vertical velocity $v(y_0, z)$ component while the horizontal velocity component is close to zero, i.e. $w(y_0, z) \approx 0$. Similarly, the vertical line of the velocity field at the vortex center will contain mainly the horizontal velocity component $w(y, z_0)$ while the vertical velocity component is close to zero, i.e. $v(y, z_0) \approx 0$. The vortex center position can be refined searching the position where velocity profiles cross zero lines, $v(y, z_0) = 0$ and $w(y_0, z) = 0$. Figure 3 shows an example of this refinement procedure. A single-component velocity profile in horizontal or vertical direction is used and the initial position of the vortex from the rough estimate using Q criterion is marked. Then a nearest zero-crossing point is found and the vortex center position is adjusted. A new radius, R, is extracted using the maximal distance between two neighbor maxima of v in z direction (i.e. where $\partial v/\partial z = 0$).

Figure 4 show an example of the vortex detection for the experimental case of $VR = 4$. In this figure a center of each vortex is marked by a cross and a circle surrounding it denotes the size of a vortex.

The last step in the characterization method is to quantify the circulation. We can transform the Cartesian grid to polar coordinates for each vortex separately, using its center and the radius, arriving at the tangential velocity u_θ

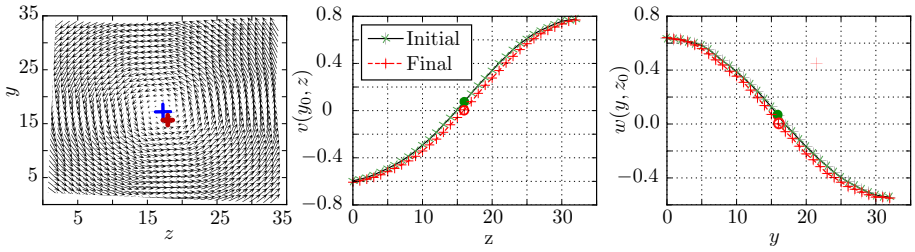

Figure 3: Refinement procedure on the localization of the vortex center (y_0, z_0), on the in-plane vector field marked by a cross (top), on the vertical velocity component at the vortex center $v(y_0, z)$ marked by a blue round (left) and on the horizontal velocity component at the vortex center $w(y, z_0)$ marked by a blue round (right). Initial and final localization of the vortex center in the refinement procedure are indicated by full and empty symbols, respectively.

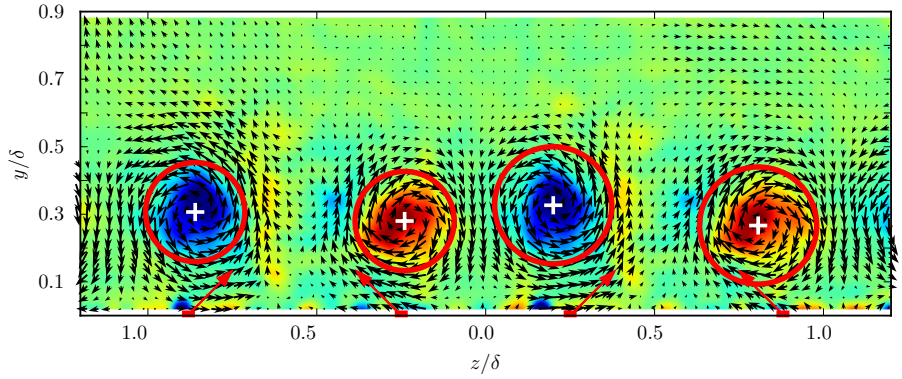

Figure 4: Isocontour of the mean streamwise vorticity Ω_x ($VR = 4$, 100 samples) with the in-plane vector field (v, w) superimposed. The extracted radius (red circle) and center of vortices (white crosses) are also superimposed. Red arrows at the wall represents controlled jet locations and orientations.

and the radial velocity u_r, as well as average streamwise vorticity Ω_x. The circulation can be computed using the integration in the polar coordinates:

$$\Gamma = \int_{\theta=0}^{\theta=2\pi} \int_{r=0}^{r=R} \Omega_x(r,\theta)\, r dr\, d\theta \tag{5}$$

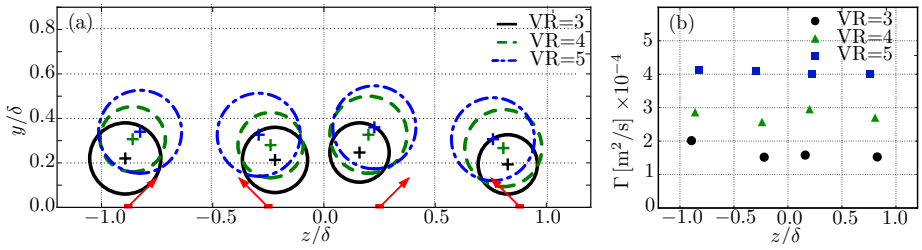

Figure 5: Effect of VR on vortex properties. (a) Location and radius of each produced streamwise vortex. Red arrows at the wall represents controlled jet locations and orientations. (b) Circulation of the vortices, Γ versus their horizontal position, z/δ.

Results in figure 5 show how vortex properties (y_0, z_0, R, Γ) vary with the control signal, VR. Vortices are shown to be displaced further from the wall (increasing y_0) with increasing VR, shift in the direction of the jet in z direction and larger circulation, Γ. The radius of the produced vortices in figure 5a, as well as the circulation in figure 5b, are shown to increase with VR. This trends of the results are in a good agreement with the results of previous studies on active device effects (e.g. [6]).

4.2. Characterisation in an instantaneous flow field

The fastest real-time processing using PIV fields, will use instantaneous PIV realisations. Figure 6 exemplifies major differences between the mean vector field for which the algorithm performs well (figure 4) and the instantaneous vector field example from the dataset of $VR = 4$. Differences between mean and instantaneous fields are obvious and the interaction of the control jet with the turbulent boundary layer flow is clearly visible in the bottom plot of the figure 6. Note that in this figure the background color represents the velocity magnitude with the low velocity region between the vortices in each pair and high velocity above the vortices.

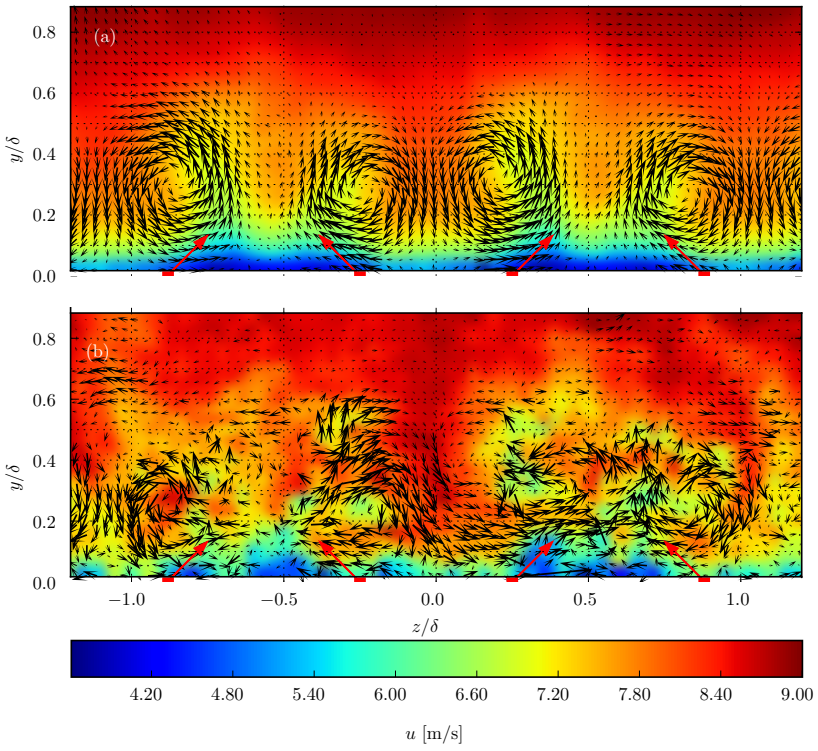

Figure 6: Isocontours of the streamwise velocity u ($VR = 4$, 100 samples) with the in-plane vector field (v, w) superimposed. Red arrows at the wall represents controlled jet locations and orientations. (a) the mean field and (b) the instantaneous field.

We address the challenge for implementation of the present identification method to instantaneous vortices, using the algorithm described in the section 4 by steps. It should be noted that streamiwe vortices generated from a jet/turbulent boundary layer interaction is a very complex turbulent flow as highlighted in Peterson *et al* [5] for jets perpendicular to the wall. It is not intented in the present work to get a full description of this flow, but rather to exploit at best instantaneous fields to get a fast estimate of the control strenght. Therefore, before computation of the Q criteria, some operations were performed on the in-plane velocity components. Firstly, the edges of the PIV field are trimed because they are generally much more noisy than the rest of the field due to loss of particles between the two PIV image pairs. Then a median filter, generaly used to denoise images, has been applied with a window size of 7. The idea behind it is to replace the ensemble average by spatial filtering on instantaneous fields, so that the vortex properties can be evaluated using a limited number of sample, which reduces the time step of the control algorithms. Also, this procedure attenuates significantly the peak locking. An example of this treatments are shown in figure 7.

The gradients are first computed using a second order accurate central differences in the interior points and first order accurate (forward or backwards) differences at the boundaries. The longitudinal vorticity Ω_x and the Q criteria (using only in-plane velocity components) are then computed. A Gaussian filter is applied on the Q criteria field, an example of results is plotted in figure 8. The vortex center is then extracted from the maximum of the Q criteria. This center estimation is reported on the raw velocity vector field, then an extraction of the vortex is performed, based on a radius roughly estimated from the filtered vorticity sign. The refinement procedure to localized the vortex center is then applied as explained in section 4.1. The vortex radius is then refined by taking the two extremum of the smoothed vertical velocity components on the horizontal line passing through the vortex center location. Once the center and the radius is defined, a Cartesian to polar transformation is performed similarly as described in diagram 3. This procedure is succesfull in 84% of the total cases

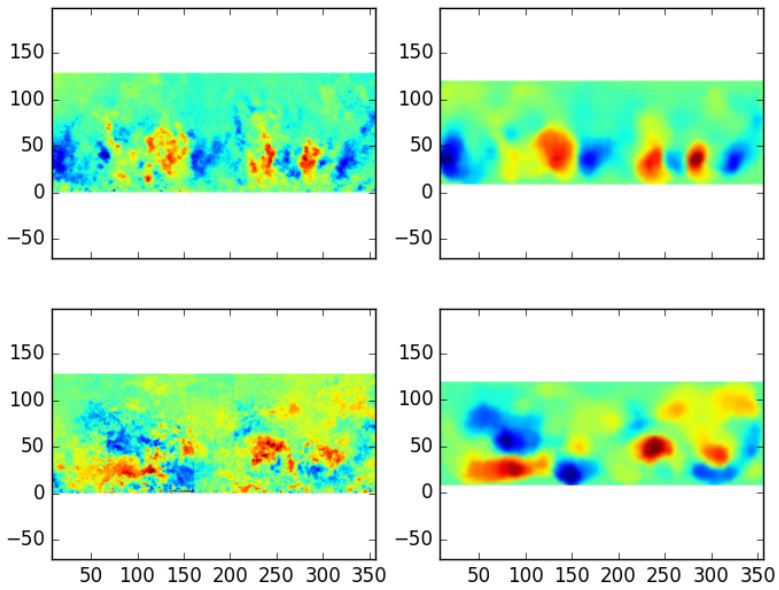

Figure 7: Example of pre-traitements before computation of Q criteria. Isocontours of the velocity component: raw v (top-left), filtered v (top-right), raw w (bottom-left), filtered w (bottom-right).

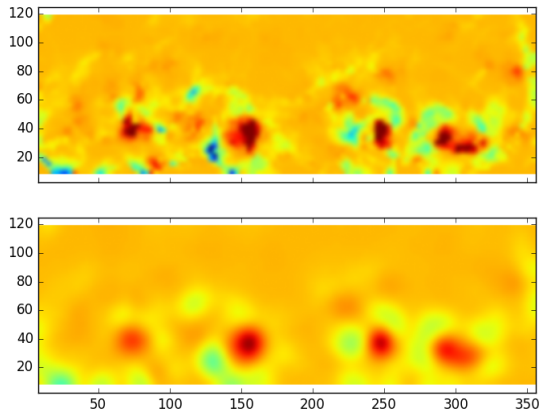

Figure 8: Example of pre-traitements of Q criteria before the peak detection. Isocontours of Q: raw (left), filtered (right).

(tested over 500 samples, see the sensibility analysis performed in section 4.3), such as an example in figure 9a. The procedure is found to fail in some cases because of the complexity of the jet/turbulent boundary layer interaction, which do not necessarily produce four dominant vortices of similar strenght near the jet exit at each instant, as shown as an example in figure 9b. Some errors such as an identified object at $y/\delta \approx 0.6$ are easily filtered out using the locations of other vortices. However, around $z/\delta \approx -0.9$, two peaks of the Q criteria are detected at the position of an expected single vortex.

The identification algorithm based on the Q-criteria is therefore not sufficiently robust for instantaneous flow fields. Although it is possible to add some ad-hoc heuristics that allows the controller to work with noisy and wrong identifications, we propose to improve the situation using a moving averaging on PIV realizations, which acts as a low-pass filter. We demonstrate in the following the effect of a moving window average of a small number of instantaneous PIV realizations on the robustness of the method.

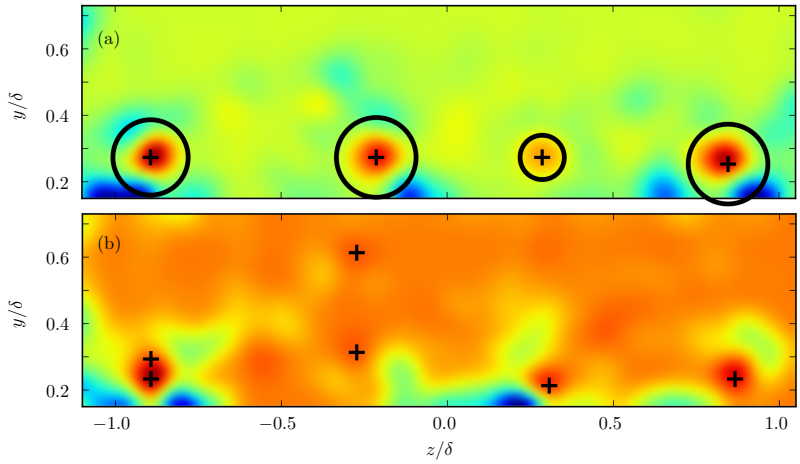

Figure 9: Examples of application of Q criteria-based identification algorithm to two instantaneous fields with crosses that indicate maxima locations from two examples: a) correct identification example from a set of $VR = 4$, b) unsuccessful example from a set of $VR = 3$.

4.3. Moving average window effect

In the present dataset, we find empirically that 10 samples moving window average provides sufficiently robust vortex detection. We present the results of the algorithm applied to a single (instantaneous), 10-sample and 100-sample averaged fields in figure 10. Figure 10a shows the detected positions and radii of the vortices for the increasing number of samples (solid - 1, dashed - 10 and dotted - 100 samples).

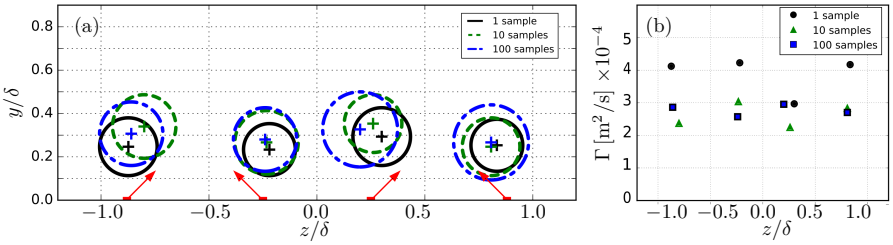

Figure 10: Average effect on the detected vortex properties, using different number of samples: (a) location and radius, (b) circulation.

The detected parameters y_0, z_0, Γ change in a non-linear fashion with the

number of samples and not equally for the four vortices. The size of the vortices, R, is larger for the case of average flow fields. Circulation of the vortices is shown in figure 10b to increase with instantaneous samples, but the results for 10 and 100 samples are comparable. As will be presented below with a more representative statistics number, the circulation is in fact decreasing with instantaneous samples. It is noteworthy that the circulation amplitude differences do not matter for closed-loop purposes, because the off-line calibration of control gain based on the measured associated lift increase for given vortex parameters will be performed with the same moving window averaging and the same number of samples.

In order to quantify the sensitivity of the results to the moving averaging procedure, we repeatedly applied the robust vortex detection algorithm on a larger dataset of 500 samples, averaged over a sliding sample window of different lengths: 1, 10 and 100. The results are presented as a spread of the quantitative results (in a form of error bars of one standard deviation) around the respective mean values in figure 4.3. It is clear also from the sensitivity analysis that the averaging window of 10 samples is sufficient to reduce the deviations to the same level as the 100 sample average with a minor compromise on the computational speed. If the vortex center is the only control parameter, then also a single PIV realization is sufficient, but the vortex radius and circulation estimates require at least the 10 samples average. The vortex radius is always higher than instantaneous detection when using block length 10/100, but in all cases the bias on averages is approximately 0.04δ, which is not significant for the control purposes.

In addition, the method was applied to test the robustness of the choice of the Q criterion threshold. To that end we start in all cases (1, 10, and 100 samples averaging) with an arbitrary chosen threshold of $Q = 0.5$ (dimensionless) and after a first pass of vortex identification the threshold is either raised or lowered according to the number of identified vortices. Because one expects 4 vortices, the second pass is performed with larger/smaller Q criterion value. Although this will require an additional computational time, the two-pass method

improves the detection from 14% to 47% for the single window sample and from 67% to 93% for the 10-sample average. For the 100-sample (almost an average flow field) it is 100% already at the first pass. For 10-sample average we were able to detect all vortices successfully with additional pass (up to 5) and an automatic treatment of the double peak of Q. For single window sample, the detection algorithm was successful at the best for 84% of the total samples and with, for some cases, up to 8 passes. In addition to double peaks of Q and very low signal to noise levels, some instantaneous fields do not show four vortices, which causes the detection to fail whatever the algorithm.

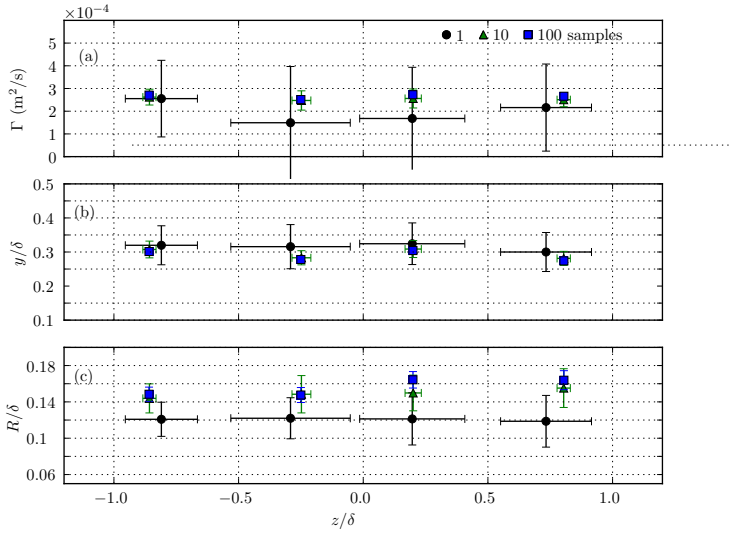

Figure 11: Sensitivity analysis of the robust method using mean and standard deviation (error-bars) of the vortex properties using 500 samples. (a) circulation, (b) vortex center positions, (c) radius. The dots are for the 1 sample window, triangles for 10, and squares for the 100 sample window averaging.

The time needed to extract the information of circulation from one instantaneous sample is arround 1.875 second. In case of windows moving average, the time to acquire n samples ($n = 10$ at minimum) should be added, this lead to a minimum of 2.71 seconds to extract the vortex circulation for the presented

example. Real time closed loop control might require identification methods that are faster than the one based on Q criterion, presented in Section 4. The method should be based on spatial velocity information, but provide a shorter sensing and identification time. The robust identification method defined in figure 2 successfully identifies the vortices based on velocity gradients. Therefore it requires 2D spatially resolved velocity field. To reduce the computation time, we tried to reduce the spatial resolution required for the velocity gradients field (coarse graining the PIV analysis). However, any compromise of the spatial resolution reduced significantly the quality of identification and is found to be non feasible.

We developed an ad-hoc vortex identification and characterisation method as explained below. This algorithm provides an order of magnitude gain in computational time and can be easily parallelised.

5. Scanning velocity profiles method

The central concept of the new method is to identify a vortex and characterize it without computing the spatial velocity gradients from PIV flow field realizations. The method based on spatial velocity gradients requires both the high spatial resolution and significant computational time. Finite difference numerical schemes are also known to amplify noise Because we identify vortices of a known orientation in a specific type of a flow field, we can develop an ad-hoc algorithm that use only horizontal (spanwise) vertical velocity component profiles, $v(z)$. These are the same type of the velocity profiles that were used in the refinement procedure as shown in figure 3.

5.1. A "line to line" PIV computation

We base our ad-hoc method on several assumptions regarding the streamwise vortices that we try to locate and characterize: a) streamwise vortices have a finite size which is smaller than the thickness of the boundary layer, b) the vortices are located close to the wall. Finite size of the vortices means that we

can save the computation time by reducing the spatial resolution and processing PIV along horizontal lines and with large vertical gaps. We demonstrate the feasibility using horizontal profiles of the vertical velocity $v(z)$. We use horizontal profiles crossing the vortex center $v(z_0)$. For the demonstration purposes we use a benchmark data of a simple vortex with major vorticity component in the out-of-plane direction, available from the PIV Challenge [23]. We analyze the data using OpenPIV [24] and the demonstration results are shown in figure 12. In this figure the arrows represent the velocity field of a cross-section of a vortex with color-coded values.

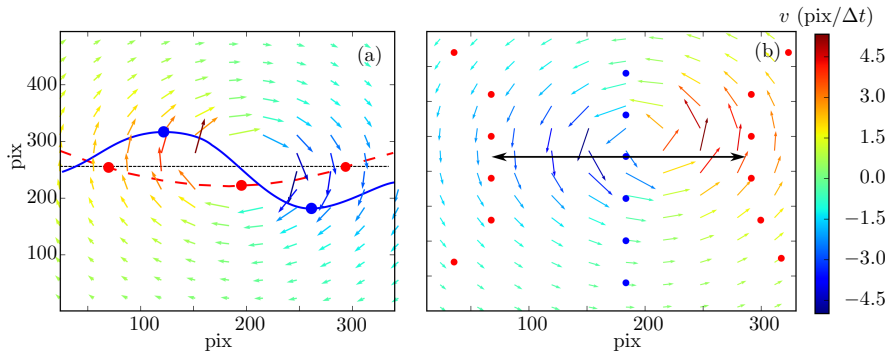

Figure 12: Demonstration of the vertical velocity identification method, using vector field of a vortex from a PIV Challenge test case. (a) Arrows denote the vector field, color of the arrows and the color scale correspond to the magnitude of vertical component, $v(y, z)$. Solid (blue) line is a horizontal velocity profile $v(y_0, z)$ at the line that corresponds to the vortex center, dashed (red) curve is a smoothed horizontal derivative $\partial v/\partial z(y_0, z)$. Dots mark the extrema and the zero crossings of $v(z)$ or of the derivative $\partial v/\partial z$. (b) Symbols marking the zero crossing and the extrema position at several horizontal positions below and above z_0. The horizontal size of a vortex is marked by the black line at the position where the distance between the crossing points is minimal.

The vertical velocity profile $v(y_0, z)$ crossing a vortex through its core is a double-peak curve. This curve is shown by a solid (blue) curve in figure 12a. We add for clarity the dots that mark the two peaks (maximum and minimum) and the square marker that emphasizes the zero crossing. It is also useful to observe the spatial derivative of the horizontal profile $\partial v/\partial z|_{y_0}$, shown as a red dashed

curve in figure 12a. This curve has a single extrema (maximum or minimum depends on the direction of the vortex axis) and the two zero-crossing points, see figure 12 The purpose of our method is to scan the velocity profiles starting from the wall and find the profiles that match the presented pattern. If we apply the peak detection method to the given flow field of a vortex at steps smaller than the presumable vortex radius, we arrive at the detection as shown in figure 12b. In this case the algorithm can find the center of a vortex without crossing it precisely, but searching for a minimal distance between the two peaks locations as emphasized by an arrow in figure 12b. This distance provides an estimate for the size of a vortex, R and the position of its center y_0, z_0. To summarize, this simple ad-hoc method allows for a very fast implementation using coarse PIV flow field.

Circulation Γ can be approximated using the integral of $\partial v/\partial z$ along the horizontal line crossing the vortex center. In the Q-criterion method, the vortex circulation, Γ, is defined as follows:

$$\Gamma = \int_{S_{vort}} \left(\frac{\partial w}{\partial y} - \frac{\partial v}{\partial z} \right) dS_{vort} \tag{6}$$

with S_{vort} the surface delimited by the vortex radius. For the proposed ad-hoc method, Δw is close to zero along horizontal lines crossing the vortex center. Therefore the strength of the vortex can be approximated using only a single component Γ_y:

$$\Gamma(\Delta y) = \Gamma_y \simeq - \int_{z_0 - R}^{z_0 + R} \frac{\partial v(y_0, z)}{\partial z} \, dz \tag{7}$$

with $v(y_0, z)$ the line profile of the vertical velocity crossing the vortex center and end points for integration on the left/right side of the vortex or $z_0 \pm R$.

The time consumption of this analysis is substantially smaller compared to the Q-criterion identification method. The method is "embarrassingly parallel" because every line in the scan can be processed separately and peak detections performed independently of the other lines. It is possible to further reduce the computation time using a 1D FFT analysis only, approximating the v component, instead of two 1D FFT runs used for the full PIV vector analysis for v, w.

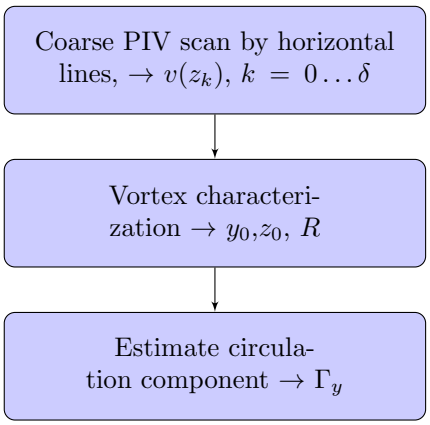

Figure 13: Diagram of the algorithm developed to extract the vortex properties (localization (y_0, z_0), radius R and circulation Γ), of produced vortices behind active vortex generators.

Furthermore, we could run the method using only a pixel-displacement version, saving time on sub-pixel peak search. The method could not become as accurate as the robust identification method. Nevertheless, it could be the only feasible solution for the very fast control applications in terms of the computation load. The computational gain of this method is inversely proportional to the size of a vortex in units of interrogation windows (IW). For instance if a vortex is $N \times M$ IW, then a single horizontal profile requires only M IWs and the gain is equal to N which in the tested case is of the order of $\sim \mathcal{O}(10)$.

5.2. Application to the dataset

For sake of comparison with the Q criterion method, we use the same 10 samples moving window averaged PIV velocity fields produced behind active vortex generators for $VR = 4$. An example of the velocity field is shown in the top panel of Figure 14. The color background is of the vertical velocity, $v(y, z)$ with blue regions marking down-wash and red regions up-wash motions. We can identify in these patterns the sides of the streamwise vortices moving fluid up/down around them. Note that the two down-wash regions between the two vortices around $z = 0$ have merged together in a single region (blue). The bottom panel demonstrates the profile of $v(z)$ (solid curve) and its horizontal

derivative, $\partial v/\partial z$ (dashed curve), at the height of an approximate center of the four vortices (the centers of each vortex are at different heights). Separate vortices can be identified as portions of the horizontal velocity profile that resemble a double-peak and zero crossing at a vortex center (as we demonstrated in figure 12).

Using the pattern of a vertical velocity profile of a vortex we identify an extrema and two neighbor zero-crossing points (marked as symbols along the zero axis) on the $\partial v/\partial z$ profile, shown by a dashed (red) curve in figure 14. The size of the vortex is then estimated as the distance between the two zero crossing points (marked as blue triangles). For the clockwise vortex the definitions are mirrored, and the algorithm searches for alternating maxima and minima of the derivative.

If the number of large peaks is higher than four (for the given case), the algorithm keeps the four strongest vortices using the magnitude of the extrema of $v(z)$.

Testing for robustness of the velocity profile based method to scanning steps we use the profiles at different heights. In this particular case we tested the sensitivity of the method if the scanning line was at different y/δ, between 0.2 to 0.4. The algorithm detects the centers of vortices also from the profiles that are off-center (not shown here). This vortex detection part of the algorithm based on the vertical velocity profile is three times faster than the Q criterion method.

5.3. Noise effect

Figure 15 shows the effect of noise for $VR = 4$ on the identified vortex properties, Γ_y, y/δ, R/δ, from the line detection method. A random noise proportional to the maximum value of the vertical velocity is added to the original signal using a different values of the coefficient k as follows:

$$v(z, y_0) = v(z, y_0) + \epsilon_v$$

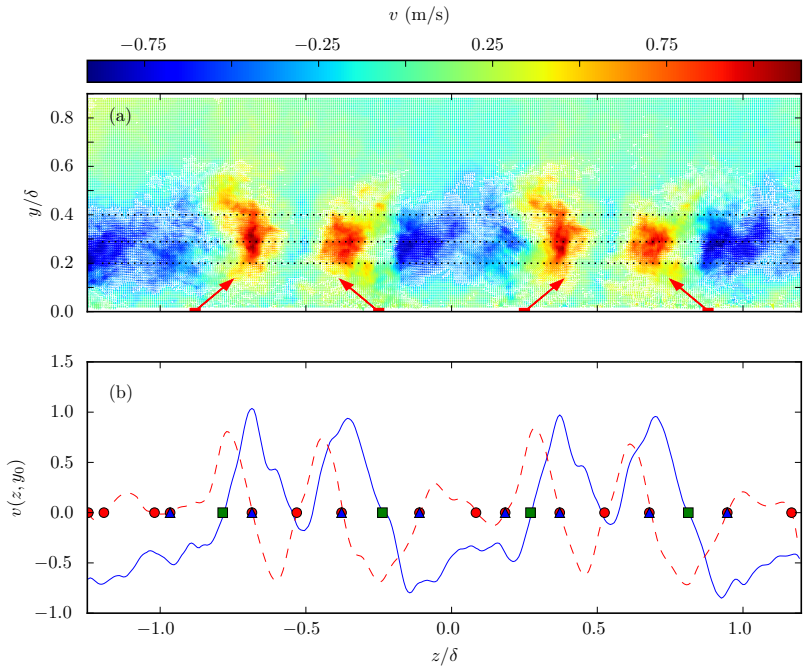

Figure 14: (top) Instantaneous velocity field for $VR = 4$, averaged over 10 samples, color map corresponds to the vertical velocity values. (bottom) Velocity profile $v(z)$ (solid curve) and its horizontal derivative $\partial v/\partial z$ (dashed curve) for the line of $z = 0.3$, an example of the vortex detection using the horizontal profile. Green squared, red dots and blue triangular mark vortex centers, zero crossings and zero-crossings, respectively, around the vortex centers.

with ϵ_v noise defined as random signal with prescribed power spectrum and a random phase. Different shapes of the spectrum were used with the bandwidth 0.01 - 200 Hz which do not affect results. Results shown in Figure 15 are performed with a constant amplitude of the spectrum from 0.01Hz to 200Hz. We vary the amplitude of the noise from k=0 to k=60% of the maximum vertical velocity, $\epsilon_v = k \times v_{\max}$. Figure 15 demonstrates the results for various amplitudes. It is seen that the algorithm performance, at least in terms of Γ_y and the vortex center positions, is weakly affected by these noise levels. A slightly stronger effect is observed in terms of the vortex radius, see Figure 15.

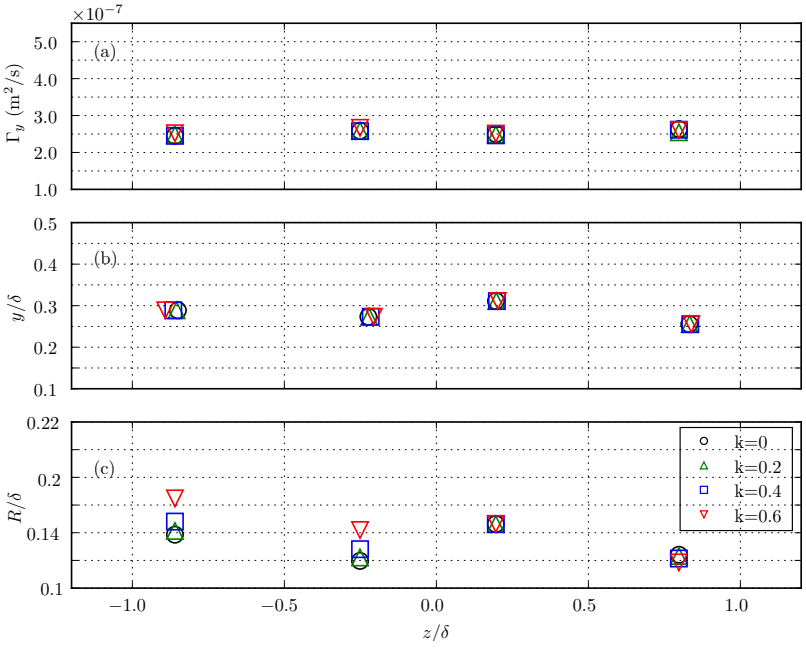

Figure 15: (a) Circulation estimate Γ_y, (b) vortex center y/δ and (c) radius R/δ identified using a velocity profile scanning method, as a function of increasing noise amplitude, k in the range of 0 - 0.6.

6. Comparison of the two methods

Results of the velocity profiles based detection are compared to the results of the Q-criterion detection method for three $VR = 3, 4, 5$ in figure 16. The detection of vortex centers shown in figure 16a are very close for the two methods, within 5%. This uncertainty is well within the requirements of the control application.

The second important measure required for the control purposes is a relative strength of a vortex. In the Q-criterion method we used circulation as the straightforward measure and have demonstrated its change due to the VR. For the velocity profile scanning method we can estimate another measure, an approximate Γ_y. The values are however different, because we use different definitions of the vortex size. In the former case this is a the threshold of Q criterion and in the latter case it is the distance between zero-crossing points of the velocity profile. It is important to note that for the control purposes any constant gain difference can be absorbed in the controller and off-line calibrated.

For the sake of visual comparison of the two methods we present the results of the magnitude of thousand times increased $1000 \times |\Gamma|$ and the respective magnitude of $|\Gamma_y|$ in figure 16.

A good correspondence between the two values is found for $VR = 3, 4$ as seen in figure 16. The proportionality value is not constant for the strongest injection case, $VR = 5$. In this case $|\Gamma_y|$ has not increased by the same amount as in the Q criterion result (shown above in figure 5b). We attribute this effect to the distorted patterns of the vortices for $VR = 5$ seen in figure 5: a) vortices have a distorted and less axi-symmetric shape (non circular), and b) larger vortices appear too close to each other and affect the identification of the zero-crossings. We note that the present distance between the control jets is arbitrary and for the sake of a real application the distance can be tuned to fit the desired VR levels of actuation.

The last identified vortex parameter is its radius. We retrieve the order of magnitudes of the identified radius using the robust method and the general

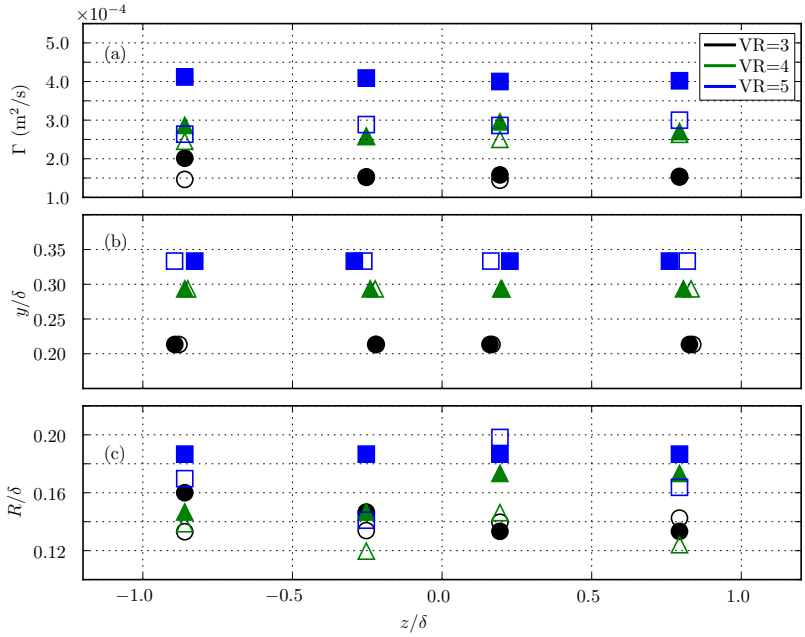

Figure 16: Results comparison between the Q-criterion based (filled symbols) and velocity profile scanning (empty symbols) detection methods: (a) $10 \times \Gamma$ compared to Γ_y, (b) position of the identified vortices, and (c) their size.

trend associated with the increase of VR, namely larger radius when VR gets higher.

One could augment and improve the velocity profile based method by estimating also a contribution in the y direction, Γ_z. This value could be estimated using the vertical profile of the horizontal velocity component, crossing the vortex center $w(y, z_0)$:

$$\Gamma(\Delta z) = \Gamma_z \simeq -\int_{y_0-R}^{y_0+R} \frac{\partial w(z_0, y)}{\partial y}\, dy \tag{8}$$

This extension of the method can solve the problem of merged vortices as they cannot merge in the vertical direction, thus improving the robustness of the method.

Comparing the two methods in term of computation time needed to extract useful information of the streamwise vortices from the velocity field, the "line to line" method criterion is $3 \times N$ times faster (N is a size of a vortex divided by the size of interrogation window), which is in our case approximately 30 times faster.

7. Conclusions

In this study we describe two real-time processing methods to identify and characterize streamwise vortices generated behind active devices placed in a turbulent boundary layer flow. We demonstrate how the PIV velocity field measurements in the spanwise - wall normal planes downstream the active vortex generators can be used to measure vortex properties such as size, distance from the wall and strength.

The first method is based on the well known Q-criterion and the integration of vorticity of the vortex, arriving at its position, size and circulation, y_0, z_0, R and Γ. We develop this method for the ideal, smooth flow field case with four embedded vortices and demonstrate the sensitivity to the number of flow realizations in the average. We show that in principle the method can be used on a single, instantaneous flow field, but only with 84% certainty. A moving

average of 10 flow fields improves the result significantly and it is demonstrated to identify and accurately characterize vortices.

For the sake of parallelization and lower computational requirements we propose also an approximate characterization method that requires neither high quality spatially resolved flow field in two dimensional cross-section, nor the computationally expensive velocity gradients calculations. This ad-hoc method uses velocity profiles and detects characteristic patterns of the vortices (two peaks and a zero-crossing between them). We explained the method using a simple example and compared its performance with the Q-criterion based method for the experimental dataset.

Both methods can identify centers and characterize strengths of streamwise vortices, generated by the active vortex generators, in a turbulent boundary layer. The most important results of the paper are the robustness of the methods and their differences in term of accuracy and processing time: both methods perform robustly only when using a filter or a moving window average of a small number of instantaneous fields, the second method is less accurate but much less time consuming (3$\times$ N times faster with N the size of the vortex divided by the size of the interrogation window).

References

[1] J. Carlier, M. Stanislas, Experimental study of eddy structures in a turbulent boundary layer using particle image velocimetry, Journal of Fluid Mechanics 535 (2005) 143–188.

[2] J. Foucaut, S. Coudert, C. Braud, C. Velte, Influence of a light sheet separation on the SPIV measurement in a large field spanwise plane., Meas. Sci. Technol 25 (3) (2014) 035304.

[3] J. Lin, Review of research on low-profil vortex generators to control boundary layer separation., Progress in Aerospace Sciences 38 (2002) 389–420.

[4] T. Shaqarin, C. Braud, S. Coudert, M. Stanislas, Open and closed-loop experiments to identify the separated flow dynamics of a thick turbulent boundary layer., Experiments in Fluids 54 (2013) 1448.

[5] S. D. Peterson, M. W. Plesniak, Evolution of jets emanating from short holes into crossflow, Journal of Fluid Mechanics 503 (2004) 57–91.

[6] C. Tilmann, K. L. Langan, J. Betterton, M. Wilson, Characterization of pulsed vortex generator jets for active flow control, in: RTO AVT Symposium on "Active Control Technology for Enhanced Performance Operational Capabilities of Military Aircraft, Land Vehicles and Sea Vehicles, Germany, 2000.

[7] R. Becker, R. King, R. Petz, W. Nitsche, Adative closed-loop separation control on a high-lift configuration using extremum seeking, AIAA Journal 45 (6) (2007) 1382–1392.

[8] N. Gautier, J.-L. Aider, Control of the separated flow downstream of a backward-facing step using visual feedback, Proceedings of the Royal Society of London A: Mathematical, Physical and Engineering Sciences 469 (2160). arXiv:http://rspa.royalsocietypublishing.org/content/469/2160/20130404.full.pdf, doi:10.1098/rspa.2013.0404. URL http://rspa.royalsocietypublishing.org/content/469/2160/20130404

[9] C. Willert, M. Munson, M. Gharib, Real-time particle image velocimetry for closed-loop flow control applications, in: 15th Int. Symp on Appl. Laser Techniques to Fluid Mechanics, Lisbon, Portugal, 2010.

[10] J. Hunt, A. Wray, P. Moin, Eddies, sreams, and convergence zones in turbulent flows, Summer Program of the Center for Turbulence research (1988) 193–207.

[11] M. Chong, A. Perry, B. Cantwell, A general classification of three-dimensional flow fields., Physics of Fluids 5 (1990) 765–777.

[12] J. Jeong, F. Hussain, On the identification of a vortex., Journal of Fluid Mechanics 285 (1995) 69–94.

[13] P. Chakraborty, S. Balachandar, R. Adrian, On the relationships between local vortex identification schemes, Journal of Fluid Mechanics 535 (2005) 189–214.

[14] C. Willert, Stereoscopic digital particle image velocimetry for application in wind-tunnel flows, Measurement Science and Technology 8 (1997) 1465–1479.

[15] M. Raffel, C. Willert, F. Scarano, C. Kaehler, S. Wereley, J. Kompenhans, Particle Image Velocimetry: A Practical Guide, Springer International Publishing, 2007.

[16] J. Westerweel, On velocity gradients in piv interrogation, Exp Fluids 44 (2008) 831–842.

[17] S. Soloff, R. Adrian, Z. Liu, Distortion compensation for generalized stereoscopic particle image velocimetry, Measurement Science and Technology 8 (1997) 1441–1454.

[18] J. Westerweel, D. Dabiri, M. Gharib, The effect of a discrete window offset on the accuracy of cross-correlation analysis of PIV, Exp Fluids 23 (1997) 20–28.

[19] J. Soria, An investigation of the near wake of a circular cylinder using a video-based digital cross-correlation particle image velocimetry technique, Experimental Thermal and Fluid Science 12 (1996) 221–233.

[20] J. Soria, J. Cater, J. Kostas, High resolution multigrid cross-correlation digital piv measurements of a turbulent starting jet using half frame image shift shift recording., Optics & Laser Technology 31 (1999) 3–12.

[21] S. Coudert, J. Schon, Back-projection algorithm with misalignement corrections for 2d3c stereoscopic PIV, Measurement Science and Technology 12 (2001) 1371–1381.

[22] A. Sciacchitano, B. Wieneke, PIV uncertainty propagation, Measurement Science and Technology 27 (2016) 084006.

[23] M. Stanislas, K. Okamoto, C. Kähler, Main results of the first international PIV challenge, Measurement Science and Technology 14 (2003) R63–R89.

[24] Z. J. Taylor, R. Gurka, G. A. Kopp, A. Liberzon, Long-duration time-resolved PIV to study unsteady aerodynamics, IEEE Transactions on Instrumentation and Measurement 59 (12) (2010) 3262–3269.